Available online at www.sciencedirect.com
ScienceDirect
Journal of Solid State Chemistry 180 (2007) 940–948
JOURNAL OF SOLID STATE CHEMISTRY
www.elsevier.com/locate/jssc

Comparative high-pressure study and chemical bonding analysis of Rh_3Bi_{14} and isostructural $Rh_3Bi_{12}Br_2$

Q.F. Gu[a,*], G. Krauss[a], Yu. Grin[b], W. Steurer[a]

[a]*Laboratory of Crystallography, ETH Zurich, Switzerland*
[b]*Max-Planck-Institut für Chemische Physik fester Stoffe, Dresden, Germany*

Received 13 October 2006; received in revised form 6 December 2006; accepted 14 December 2006
Available online 27 December 2006

Abstract

The binary compound Rh_3Bi_{14} was synthesized from the elements. The compound is isostructural with $Rh_3Bi_{12}Br_2$, crystallizes with the orthorhombic space group *Fddd* (no. 70) and lattice parameters $a = 6.8959(15)$ Å, $b = 17.379(3)$ Å, $c = 31.758(6)$ Å. The crystal structure consists of a three-dimensional (3D) framework of edge-sharing cubes and square antiprisms ($RhBi_{8/2}$). It is closely related to the intermetallic compound $RhBi_4$, in which two Y-like frameworks of antiprisms interpenetrate. In Rh_3Bi_{14} and $Rh_3Bi_{12}Br_2$, additional bismuth and bromine anions, respectively, fill the channels of the 3D polyhedral framework formed by covalently bonded rhodium and bismuth atoms. High-pressure X-ray powder diffraction data from synchrotron measurements of Rh_3Bi_{14} and $Rh_3Bi_{12}Br_2$ indicate a high stability of both compounds in the investigated range from ambient pressure to ca. 30 GPa at ambient temperature.

Keywords: High pressure; Intermetallic compound; ELF; Single crystal diffraction

1. Introduction

In recent years, complex metallic alloys (CMAs) are gaining more and more interest because of potential unusual physical properties due to different length scales present in their crystal structures [1]. Group 15 metals are interesting starting elements for the preparation of new CMAs due to their versatile crystal chemistry at ambient as well as non-ambient conditions. Elemental bismuth, for example, transforms into modulated structures at pressures close to 10 GPa and is one of the most studied elements at high pressures [2]. Transition-metal bismuth compounds can be partially oxidized by halogen atoms, which leads to a wide range of compounds from 'porous' two-dimensional (3D) metals through two-dimensional (2D) and one-dimensional (1D) systems and semiconductors with very small or moderately large band gaps [3]. $RhBi_4$, for example, the crystal structure of which consists of tetragonal antiprisms ($RhBi_{8/2}$) [4,5], can be partly oxidized using bromine to form the compound $Rh_3Bi_{12}Br_2$ [6]. This compound consists of a 3D open framework (packing of ($RhBi_{8/2}$) square antiprisms and cubes) with bromine atoms filling the voids. Substituting the atoms in the voids may allow the tailoring of physical properties.

Here, we report on the synthesis and crystal structure of the novel compound Rh_3Bi_{14}, which is isostructural with $Rh_3Bi_{12}Br_2$, and contains bismuth instead of bromine atoms. The crystal structure, chemical bonding and high-pressure stability of both isostructural compounds will be compared.

2. Experimental details

2.1. Preparation

Rh_3Bi_{14} single crystals were grown by the Bi-flux method. 3 mmol Rh powder (99.9%, Goodfellow) were mixed with 20 mmol Bi powder (99.9%, Goodfellow) and pressed into a pellet in an argon-filled glove box. For homogenization, the pellet was melted three times in an arc furnace under argon atmosphere. The ingot was sealed in an evacuated quartz tube with a quartz wool filter, comparable to the setup described in [7]. It was heated

*Corresponding author. Fax: +41 44 632 11 33.
E-mail address: qinfen.gu@mat.ethz.ch (Q.F. Gu).

0022-4596/$ - see front matter © 2007 Elsevier Inc. All rights reserved.
doi:10.1016/j.jssc.2006.12.020

up to 600 °C (heating rate 10 °C/min) kept for 1 day, subsequently cooled down to 320 °C within 2 days, and followed by an annealing at 320 °C for 5 days. The quartz tube was taken out from the furnace and the residual melt was forced through the filter by centrifugation. Single crystals of Rh_3Bi_{14} were selected from the top of the quartz wool filter. These crystals have a metallic luster and are insensitive to air and moisture. The chemical composition of several single crystals has been checked by energy dispersive X-ray analysis (EDX) to be about 18(1) at% Rh and 82(1) at% Bi. No other elements were detected.

$Rh_3Bi_{12}Br_2$ was synthesized in a modified route compared to [6]. A mixture of 3 mmol Rh powder (99.9%, Goodfellow), 20 mmol Bi powder (99.9%, Goodfellow) and 2 mmol $BiBr_3$ powder (99.9%, Goodfellow) was heated in an evacuated quartz ampoule up to 900 °C (heating rate 15 °C/min) and subsequently cooled down to room temperature within 72 h. Dark brown shiny single crystals of $Rh_3Bi_{12}Br_2$ were selected from the bottom of the quartz ampoule. The byproducts were not further characterized.

2.2. X-ray diffraction

Single crystal X-ray diffraction data of Rh_3Bi_{14} and $Rh_3Bi_{12}Br_2$ were collected on an Oxford-Diffraction XCalibur XP diffractometer equipped with an Onyx CCD-detector using Mo$K\alpha$ radiation (Oxford enhance). Numerical absorption correction of measured intensities was performed by the CrysAlis RED program package [8]. Crystal structures of both compounds were solved in the space group *Fddd* (no. 70) by using ShelXS [9] and refined against F^2 using the ShelXL97 program [9].

High-pressure studies were done on powdered samples at the Swiss-Norwegian beam lines (SNBL), ESRF, Grenoble. HP up to ca. 30 GPa were generated by use of the ETH diamond anvil cell (DAC) [10]. The ruby fluorescence method was used for pressure determination. Rhenium gaskets were used and a mixture of methanol and ethanol in the ratio of 4:1 served as pressure-transmitting medium. To minimize the scattering of the gasket, the beam size was reduced to about $80 \times 80\,\mu m^2$. The diffraction data was collected on a Marresearch mar345 IP-detector using a wavelength of $\lambda = 0.70933$ Å. Integration of the 2D powder diffraction patterns was realized by means of the computer program fit2d [11]. For lattice parameters, refinement the GSAS program package [12] was used. Equations of state were calculated by the use of the program EosFit5.2 [13].

2.3. Calculation procedure

For quantum chemical calculations, the TB-LMTO-ASA program package [14] with exchange correlation potential (LDA) according to Barth and Hedin [15] was used. The radial scalar-relativistic Dirac equation was solved to get the partial waves. The calculation within the atomic sphere approximation (ASA) includes corrections for the neglect of interstitial regions and partial waves of higher order [16], hence no addition of empty spheres was found necessary. The following radii of atomic spheres were used in the calculations for Rh_3Bi_{14}: r(Rh1) = 1.682 Å, r(Rh2) = 1.671 Å, r(Bi1) = 1.844 Å, r(Bi2) = 1.872 Å, r(Bi3) = 1.872 Å, r(Bi4) = 2.240 Å; for $Rh_3Bi_{12}Br_2$: r(Rh1) = 1.726 Å, r(Rh2) = 1.719 Å, r(Bi1) = 1.931 Å, r(Bi2) = 1.898 Å, r(Bi3) = 1.906 Å, r(Br) = 1.973 Å. The basis sets containing Rh(5s,5p,4d), Bi(6s,6p) and Br(4p) orbitals were employed for a self-consistent calculation with Rh(4f), Bi(6d,5f) and Br(5s,4d) functions being downfolded.

The election localization function (ELF, η) was evaluated according to [17] with an ELF module already implemented within the TB-LMTO-ASA program package [14]. To gain a deeper insight into the chemical bonding, the topology of ELF was analyzed with the program Basin [18]. The election density was integrated in basins, which

Table 1
Crystallographic data and structure refinement for Rh_3Bi_{14} and $Rh_3Bi_{12}Br_2$[6]

Empirical formula	Rh_3Bi_{14}	$Rh_3Bi_{12}Br_2$
Formula weight	3234.45	2976.31
Temperature	295(2) K	293(1) K
Wavelength	0.71073 Å	0.71073 Å
Crystal system, space group	Orthorhombic, *Fddd* (no. 70)	Orthorhombic, *Fddd* (no.70)
Unit cell dimensions	$a = 6.8959(15)$ Å	$a = 7.1712(3)$ Å
	$b = 17.379(3)$ Å	$b = 16.8037(6)$ Å
	$c = 31.758(6)$ Å	$c = 31.871(1)$ Å
Volume	3806.1(13) Å^3	3840.6 Å^3
Z, calculated density	8, 11.289 mg/m^3	8, 10.295 mg/m^3
Absorption coefficient	131.403 mm^{-1}	116.1 mm^{-1}
Crystal size	$0.010 \times 0.010 \times 0.015$ mm^3	$0.16 \times 0.08 \times 0.04$ mm^3
Theta range for data collection	3.72–37.54°	1.5–22.5°
Limiting indices	$-10 <= h <= 11$, $-29 <= k <= 28$, $-53 <= l <= 38$	$-9 <= h <= 9$, $21 <= k <= 21$, $41 <= l <= 41$
Reflections collected/unique	9691/2423 [R(int) = 0.0695]	4958/1112 [R(int) = 0.034]
Refinement method	Full-matrix least-squares on F^2	Full-matrix least-squares on F^2
Data/restraints/parameters	2423/0/43	1112/0/43
Goodness-of-fit on F^2	0.960	1.079
Final R indices [$I > 4$sigma(I)]	$R1 = 0.0362$, w$R2 = 0.0804$	$R1 = 0.018$
R indices (all data)	$R1 = 0.0574$, w$R2 = 0.0853$	$R1 = 0.031$, w$R2 = 0.025$

are bounded by zero flux surfaces in ELF gradient. The method, analogous to the procedure proposed by Bader for the electron density [19], allows to assign an electron count for each basin, revealing basic information for the description of the bonding situation.

3. Results and discussion

3.1. The crystal structure of Rh_3Bi_{14}

Rh_3Bi_{14} is the Bi-richest binary Rh–Bi compound. It is isostructural with $Rh_3Bi_{12}Br_2$ [6]. Experimental details of the structure analysis of Rh_3Bi_{14} are summarized in Table 1. The atomic coordinates and anisotropic displacement parameters (ADP) are listed in Table 2, interatomic distances and angles are given in Table 3.

Table 2

A. *Atomic coordinates for Rh_3Bi_{14} from this study and for isostructural $Rh_3Bi_{12}Br_2$ [6] for comparison*

Atom	Site	x	y	z
Rh_3Bi_{14}				
Rh1	16*c*	0.25	0.25	0
Rh2	8*a*	0.125	0.125	0.125
Bi1	32*h*	−0.0711(1)	0.1844(1)	0.0730(1)
Bi2	32*h*	0.4937(1)	0.2451(1)	0.0719(1)
Bi3	32*h*	0.0920(1)	0.3428(1)	0.0160(1)
Bi4	16*f*	0.125	0.3442(1)	0.125
$Rh_3Bi_{12}Br_2$				
Rh1	16c	0.25	0.25	0
Rh2	8*a*	0.125	0.125	0.125
Bi1	32*h*	0.00183(5)	0.25119(1)	0.07188(1)
Bi2	32*h*	0.41509(5)	0.17797(1)	0.07198(1)
Bi3	32*h*	0.16446(5)	0.41266(1)	0.01374(1)
Br	16*f*	0.125	0.41546(6)	0.125

B. *Anisotropic displacement parameters (10^4 Å^2) for Rh_3Bi_{14} and for isostructural $Rh_3Bi_{12}Br_2$[6]*

	U_{11}	U_{22}	U_{33}	U_{23}	U_{13}	U_{12}
Rh_3Bi_{14}						
Bi(1)	159(2)	174(2)	141(1)	−25(1)	2(1)	1(1)
Bi(2)	178(2)	158(2)	148(1)	−23(1)	−17(1)	23(1)
Bi(3)	197(2)	142(1)	169(1)	−15(1)	36(1)	−6(1)
Rh(1)	182(5)	122(4)	129(3)	−10(3)	−16(4)	−5(4)
Rh(2)	159(6)	134(5)	96(5)	0	0	0
Bi(4)	470(4)	201(2)	200(2)	0	−88(3)	0
$Rh_3Bi_{12}Br_2$						
Bi(1)	172(2)	124(1)	137(1)	22(1)	24(1)	3(1)
Bi(2)	131(2)	156(1)	133(1)	−10(1)	−9(1)	20(1)
Bi(3)	161(2)	115(1)	162(1)	−3(1)	42(1)	−14(1)
Rh(1)	164(5)	109(3)	118(3)	−9(3)	36(3)	23(3)
Rh(2)	205(8)	115(5)	87(5)	0	0	0
Br	313(9)	236(5)	269(5)	0	−97(5)	0

Coefficients U_{ij} (in 10^4 Å^2) of the tensors of the anisotropic displacement parameters exp{_2p2[$U_{11}h2a$*2 _..._ 2$U_{23}klb$*c*]}.

Table 3
Selected bond lengths (Å) and angles (deg) for Rh_3Bi_{14}

Distances		Angles	
Rh(2)–Bi(2) × 4	2.8308(5)	Rh(1)–Bi(1)–Rh(2)	107.178(19)
Rh(2)–Bi(1) × 4	2.8604(5)	Rh(2)–Bi(1)–Bi(2)	55.579(14)
Rh(1)–Bi(1) × 2	2.8638(5)	Rh(1)–Bi(1)–Bi(2)	56.828(11)
Rh(1)–Bi(2) × 2	2.8897(5)	Rh(2)–Bi(1)–Bi(3)	145.316(15)
Rh(1)–Bi(3) × 2	2.9023(6)	Rh(1)–Bi(1)–Bi(3)	53.375(12)
Rh(1)–Bi(3) × 3	2.8508(6)	Bi(2)–Bi(1)–Bi(3)	92.136(16)
Bi(1)–Bi(2) × 1	3.1808(9)	Rh(2)–Bi(1)–Bi(4)	107.307(14)
Bi(1)–Bi(3) × 2	3.3016(7)	Rh(1)–Bi(1)–Bi(4)	103.444(17)
Bi(1)–Bi(2) × 2	3.3392(8)	Bi(2)–Bi(1)–Bi(4)	96.132(16)
Bi(1)–Bi(1) × 1	3.4034(9)	Bi(3)–Bi(1)–Bi(4)	59.551(15)
Bi(1)–Bi(3) × 1	3.4808(7)	Rh(1)–Bi(2)–Rh(2)	107.272(16)
Bi(1)–Bi(4) × 2	3.5020(8)	Rh(2)–Bi(2)–Bi(1)	56.463(10)
Bi(1)–Bi(2) × 2	3.6947(7)	Rh(1)–Bi(2)–Bi(1)	56.048(13)
Bi(2)–Bi(3) × 2	3.2386(7)	Rh(1)–Bi(3)–Bi(4)	103.443(13)
Bi(2)–Bi(4) × 3	3.3852(8)	Rh(1)–Bi(3)–Bi(1)	52.362(11)
Bi(2)–Bi(4) × 3	3.5035(7)	Bi(4)–Bi(3)–Bi(1)	60.528(14)
Bi(2)–Bi(3) × 2	3.5178(7)	Bi(3)–Bi(4)–Bi(1)	59.921(11)
Bi(3)–Bi(3) × 1	3.1956(10)	Bi(2)–Rh(2)–Bi(1)	67.958(16)
Bi(4)–Bi(3) × 2	3.4677(7)	Bi(1)–Rh(1)–Bi(2)	67.125(17)
Bi(4)–Bi(4) × 2	3.6100(8)	Bi(1)–Rh(1)–Bi(3)	74.263(14)
		Bi(2)–Rh(1)–Bi(3)	112.006(15)

The unit cell contains 136 atoms (24 Rh and 112 Bi) as shown in Fig. 1. There are two crystallographically independent Rh atoms in the crystal structure of Rh_3Bi_{14}. Each Rh atom is surrounded by eight Bi atoms. Rh1 is cubically coordinated, whereas Rh2 exhibits a square antiprismatic coordination. There are twice as much cubes as square antiprisms present in the crystal structure. The structure is closely related to the intermetallic compound $RhBi_4$, in which two frameworks of antiprisms interpenetrate [20]. Here, the result of the condensation of ($RhBi_{8/2}$) polyhedra is a 3D framework of edge-sharing cubes and square antiprisms with channels along the [100] direction as shown in Fig. 2. Rh_3Bi_{14} differs from $Rh_3Bi_{12}Br_2$ only by the atoms in the channels. In Rh_3Bi_{14}, Bi atoms fill the channels, whereas they are filled by Br atoms in $Rh_3Bi_{12}Br_2$.

Both structures crystallize with the same space group, *Fddd*, with slightly different lattice parameters (cf. Table 1). For Rh_3Bi_{14}, the *a* and *c* lattice parameters are smaller, but the *b* lattice parameter is larger than for $Rh_3Bi_{12}Br_2$. This is caused by a larger zigzag angle of the Bi chain in the channel of Rh_3Bi_{14} (145.54(4)°) compared to the Br chain in $Rh_3Bi_{12}Br_2$ (138.44(3)°). The interconnecting angle between the cubes and antiprisms also only differs slightly for both compounds: 60.231(12)° for Rh_3Bi_{14} compared to 58.39(7)° for $Rh_3Bi_{12}Br_2$. The geometric distortion of the cubes and antiprisms due to the different atoms in the channel is negligible (Table 3).

The displacement ellipsoid of the Bi4 atom in the channel direction of Rh_3Bi_{14} ($U_{11} = 0.0470(4)$ Å^2, $U_{22} = 0.0201(2)$ Å^2, $U_{33} = 0.0200(2)$ Å^2) is more elongated than

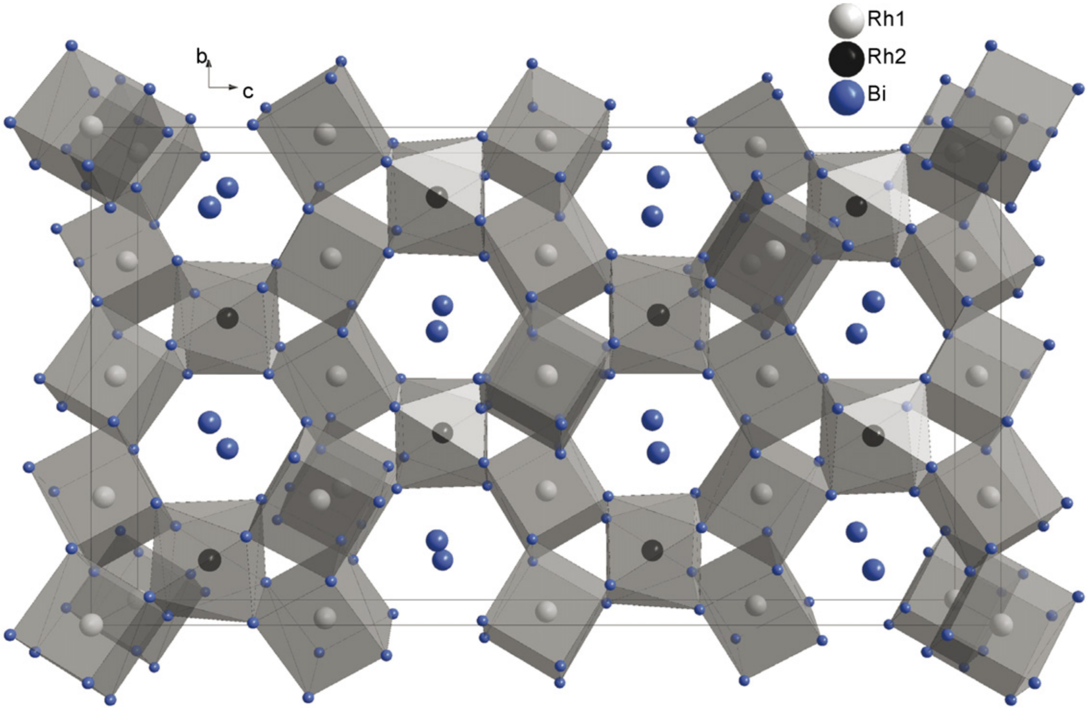

Fig. 1. Perspective view of the crystal structure of Rh_3Bi_{14}. The 3D framework is built of (RhBi8/2) cubes and square antiprisms, which share common edges. Bi4 atoms fill the channels of the framework.

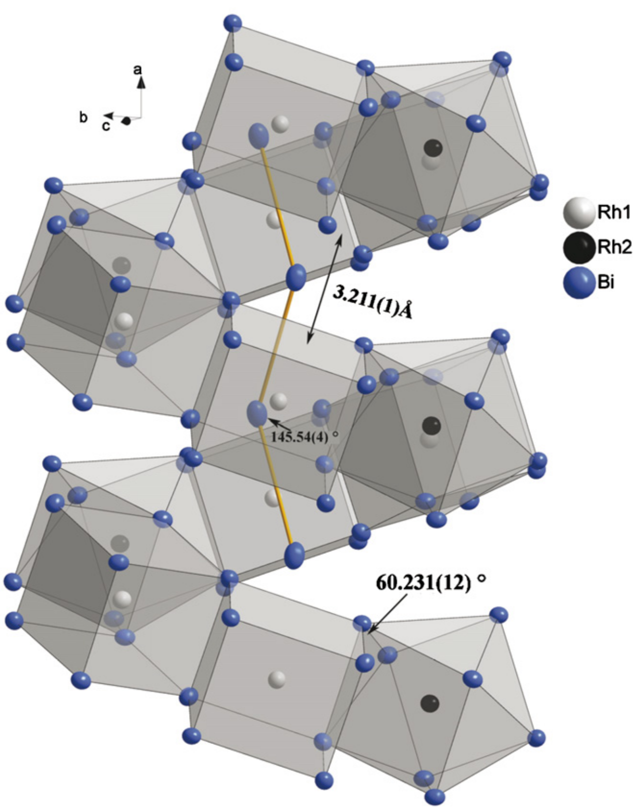

Fig. 2. The channel built of edge-sharing (RhBi8/2) cubes and square antiprisms filled with Bi4 atoms forming the zigzag channel (yellow line) in Rh_3Bi_{14}. All atoms are shown by their displacement ellipsoids.

that for Br in $Rh_3Bi_{12}Br_2$ ($U_{11} = 0.0313(9)\,\text{Å}^2$, $U_{22} = 0.0236(5)\,\text{Å}^2$, $U_{33} = 0.0269(5)\,\text{Å}^2$ [6]). The reliability of the ADP values is confirmed by the high resolution of the dataset ($2\theta > 75°$); the values are also comparable to other Bi compounds as found in the literature (e.g. [3,6]).

3.2. Chemical bonding

Despite the high complexity of the crystal structures of Rh_3Bi_{14} and $Rh_3Bi_{12}Br_2$ the electron localization function reveals only few special features, which are well positioned. The distribution of ELF in Rh_3Bi_{14} around the Bi1, Bi2 atoms shows two attractors for each atom and for Bi3 one attractor in the valence region (Figs. 3a–d). They are positioned on the outer side of the Bi–Rh contacts and are monosynaptic, i.e. their basins contact only the own core regions. This allows to interpret them as the 'lone-pair' attractors. The 'lone pairs' are located in the 'empty' space between the cubes and antiprisms ($RhBi_{8/2}$). Thereby, the Bi–Rh contacts and the 'lone-pair' attractors lie nearly in one plane and not in a tetrahedral arrangement, expected from the fact that each atom Bi1, Bi2 or Bi3 interconnects two rhodium atoms (cf. Table 2), i.e. may form two bonds and two lone pairs. The same topological features of the ELF are observed around the Bi1, Bi2 and Bi3 atoms in the crystal structure of $Rh_2Bi_{12}Br_2$ (Fig. 4a).

The valence shell of the bromine atoms in the crystal structure of $Rh_3Bi_{12}Br_2$ (Fig. 4b) is nearly spherical. No additional attractors were found in vicinity of Br. This

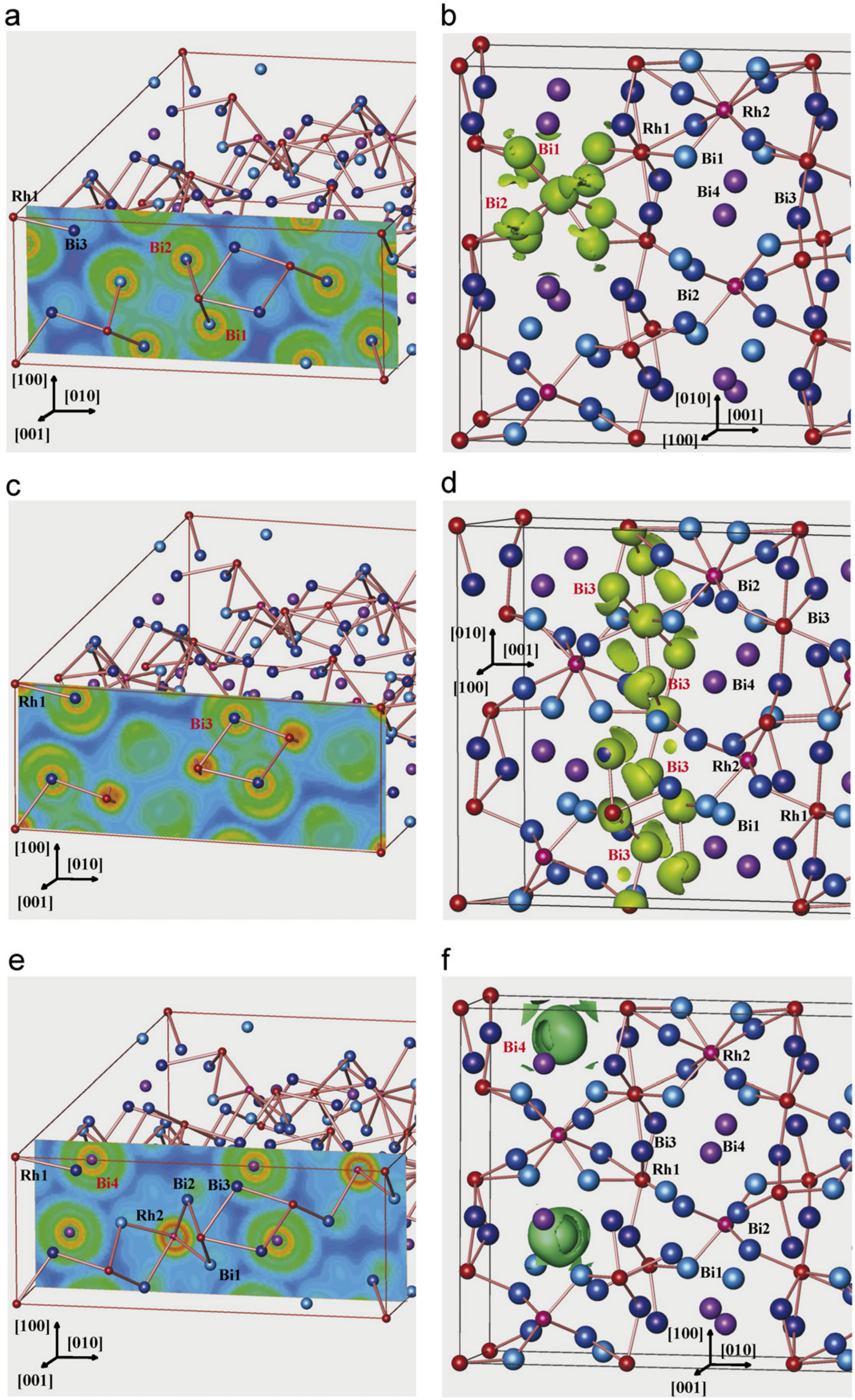

Fig. 3. Electron localization function for Rh_3Bi_{14}: (a) section through the Bi1 and Bi2 atoms; (b) isosurface of $\eta = 0.455$ in vicinity of Bi1 and Bi2 atoms; (c) section through the Bi3 atoms; (d) isosurface of $\eta = 0.48$ in vicinity of Bi3 atoms; (e) section through the Bi4 and Rh2 atoms; (f) isosurface of $\eta = 0.36$ in vicinity of Bi4 atoms.

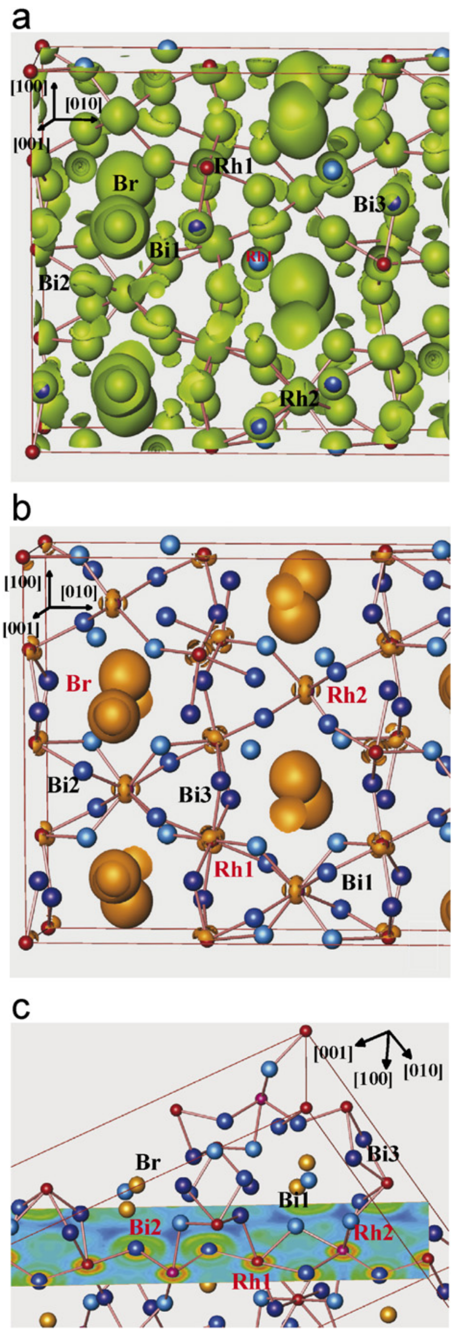

Fig. 4. Electron localization function for $Rh_3Bi_{12}Br_2$: (a) isosurface of $\eta = 0.48$; (b) isosurface of $\eta = 0.73$ in vicinity of Br and Rh atoms; (c) section through the Bi1 and Rh atoms.

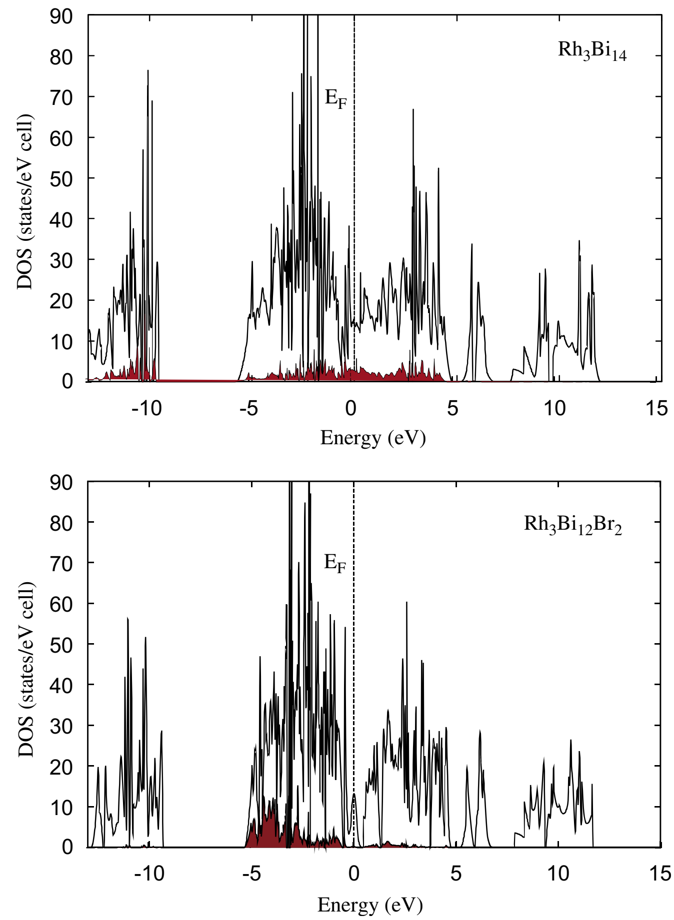

Fig. 5. Electronic density of states for Rh_3Bi_{14} and $Rh_3Bi_{12}Br_2$. Contributions of the Bi4 s and p and of the Br s and p states are shown in red.

suggests the close-shell configuration of bromine (i.e., Br^{1-}) in agreement with the electronic density of states, which shows practically all s and p states of the bromine occupied (Fig. 5). The valence shell of the Bi4 atoms in the crystal structure of Rh_3Bi_{14} (Figs. 3e and f) is slightly more deviating from the spherical shape comparing to the situation around bromine. This is also in agreement with the electronic density of states (Fig. 5), which reveals a part of the p states unoccupied and suggests the small negative charge for the Bi4 position (Bi^{1-}).

The distribution of the ELF in the region of the penultimate shell of the rhodium atoms in both crystal structures, Rh_3Bi_{14} (Fig. 6a) and $Rh_3Bi_{12}Br_2$ (Fig. 4b), shows a characteristic structuring already observed for transition metal atoms in molecules [21] and suggests the participation of the electrons of the 4th shell (d electrons) in the bonding. The ELF attractors in vicinity of the Rh–Bi contacts are very low pronounced (the maximum value of η deviates from the next interconnecting point by less then 0.01), but are located in the expected regions (Figs. 4c and 6b), i.e. they can be understood as a part of an expected ring attractor around the Rh–Bi contact. For comparison, see Sc–Ge bonding [21]. The less pronounced attractors are caused by the fact that the contributions of the d electrons to the total ELF are smaller on the absolute scale comparing with the s and p electrons [22].

The calculated electronic density of states (Fig. 5) shows non-zero values at the Fermi level for both compounds suggesting metallic behavior for the electronic transport properties. In this region, the DOS is formed mainly by the p states of bismuth and d states of rhodium atoms. Slightly above the Fermi level, a small gap is formed in the DOS for $Rh_3Bi_{12}Br_2$ (Fig. 5, bottom), which is not observed in

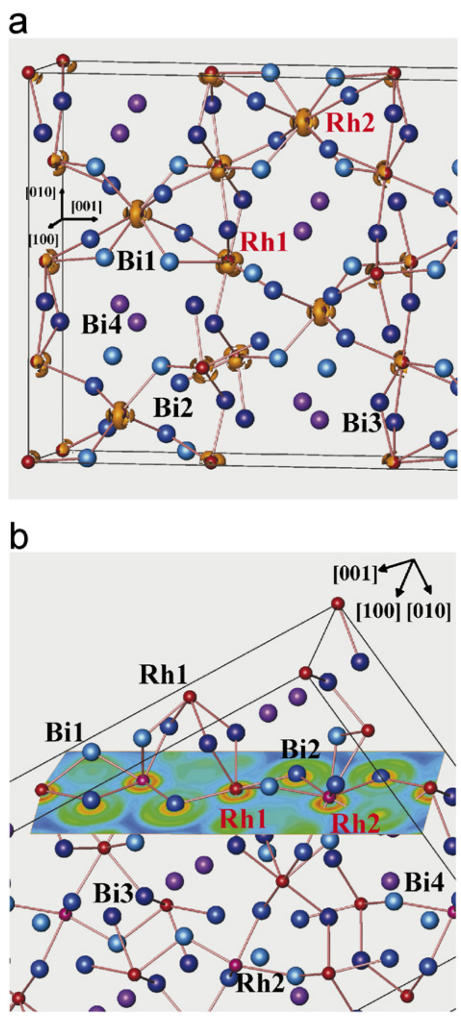

Fig. 6. Electron localization function for Rh_3Bi_{14}: (a) isosurface of $\eta = 0.73$ in vicinity of Rh1 and Rh2 atoms; (c) section through the Rh and Bi1 atoms.

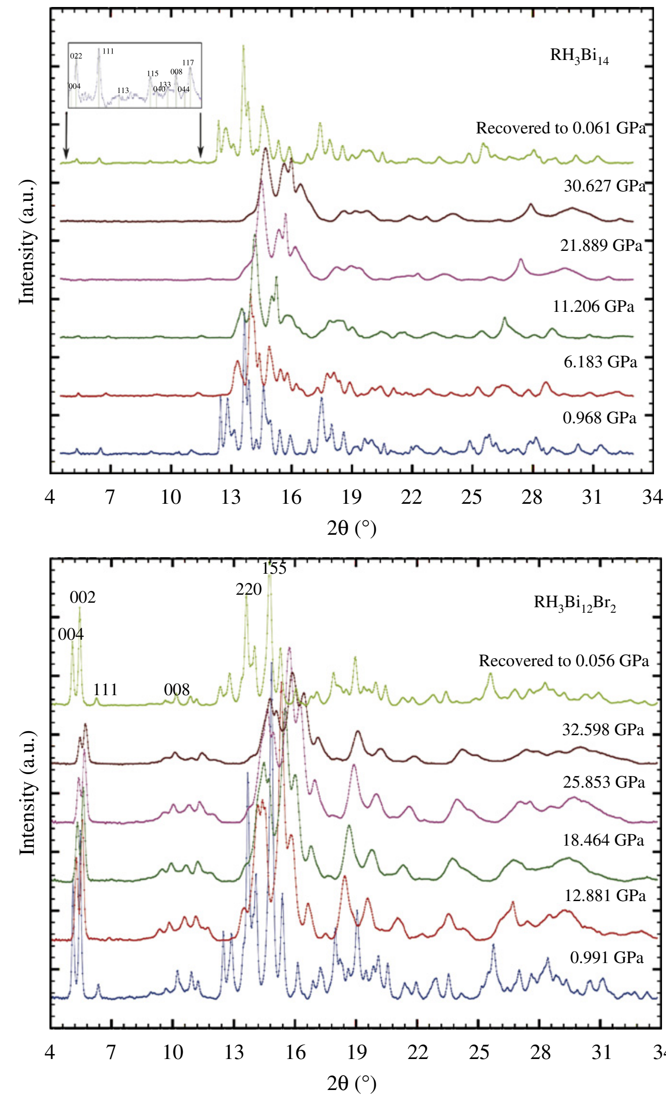

Fig. 7. X-ray powder diffraction patterns at different pressures. The enlarged section in the inset shows the well-separated peaks at small diffraction angles.

Rh_3Bi_{14}. This is to understand in sense of smaller contribution of the bromine compared with the Bi4 to the vicinity of Fermi level.

Despite the small differences in the electronic DOS, from the ELF representation in total, the crystal structures of Rh_3Bi_{14} and $Rh_3Bi_{12}Br_2$ can be understood as covalently bonded 3D polycations $[Rh_3Bi_{12}]^{2+}$ forming the channels, which are occupied by the Bi^{1-} or Br^{1-} anions, which, even if they are chemically differences, are playing the same role in the atomic interactions. Because there are no directed bonds between the polycation and anions, the latter have additional freedom for the moving inside the channels which find the expression in the pronounced anisotropy of the atomic displacement (cf. Chapter 3.1). The size of the bromine anion is larger than that of the bismuth one. This causes the increase in the unit cell volume from Rh_3Br_{14} to $Rh_3Bi_{12}Br_2$. The volume increase is caused by the larger bromine contributions to the *a* and *c* lattice parameters, but not to the *b* parameter. The zigzag angle (cf. Chapter 3.1) is not defined by a directed covalent bonding, but by the ionic interaction. Thus, its value is a result of a packing effect more than by two-center Bi–Bi or Br–Br interactions.

3.3. High-pressure studies

Owing to the identical 3D framework, but different atom types in the channels, it is interesting to study the behavior of the crystal structures Rh_3Bi_{14} and $Rh_3Bi_{12}Br_2$ as a function of pressure. To our knowledge, no high-pressure studies on transition metal bismuth compounds were known to the literature so far.

Fig. 7 shows some representative powder diffraction patterns obtained from synchrotron measurements. Because of the severe line broadening caused by internal strain combined with strong peak overlay due to the large lattice parameters, no structural refinements could be done

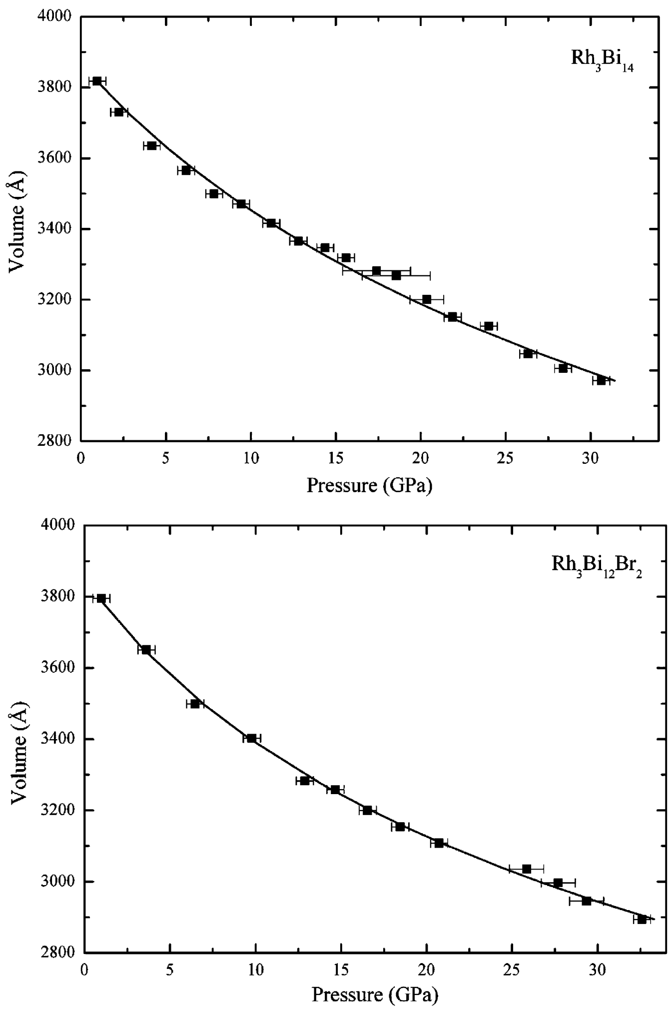

Fig. 8. Unit cell volume of Rh_3Bi_{14} and $Rh_3Bi_{12}Br_2$ as a function of pressure. The solid line corresponds to a 2nd-order Birch–Murnaghan equation of state (Table 4). with a bulk modulus $K_0 = 70(5)$ GPa and $K_0 = 67(4)$ GPa for Rh_3Bi_{14} and $Rh_3Bi_{12}Br_2$, respectively. The errors of the volume are in the size of the symbols.

at higher pressures. Except the broadening, no drastic structural changes of the diffraction pattern were observed up to the highest reached pressures, 30.6 GPa for Rh_3Bi_{14}, and 32.6 GPa for $Rh_3Bi_{12}Br_2$, respectively. After pressure release, the observed patterns are comparable to those collected before the high-pressure study. The lattice parameters for both phases were refined using the Rietveld method with fixed structure parameters. The presence of non-overlapping reflections at small scattering angles assures reliable refinements (see inset in Fig. 7). A 2nd-order Birch–Murnaghan equation of state $P = (3K_0/2)(((V_0/V))^{7/3} - (V_0/V)^{5/3})$ was fitted to the experimental data (Fig. 8, Table 4). The large uncertainties of the data points for Rh_3Bi_{14} between 15 and 20 GPa is caused by a new loading of the DAC.

Both structures were generally stable within the framework of the experiment. The axes of both phases behave different as a function of pressure. The zero-pressure

Table 4
Summary of zero pressure volume V_0, zero-pressure bulk modulus K_0, and the zero-pressure compressibility β_0 of the *a, b, c* lattice parameters for Rh_3Bi_{14} and $Rh_3Bi_{12}Br_2$

Compound	V_0 (Å^3)	K_0 (GPa)	$\beta_0 a$ (GPa^{-1})	$\beta_0 b$ (Gpa^{-1})	$\beta_0 c$ (GPa^{-1})
Rh_3Bi_{14}	3867.59	70 (5)	−0.0063(3)	−0.0073(3)	−0.0066(6)
$Rh_3Bi_{12}Br_2$	3819.78	67 (4)	−0.0152(2)	−0.0015(5)	−0.0026(6)

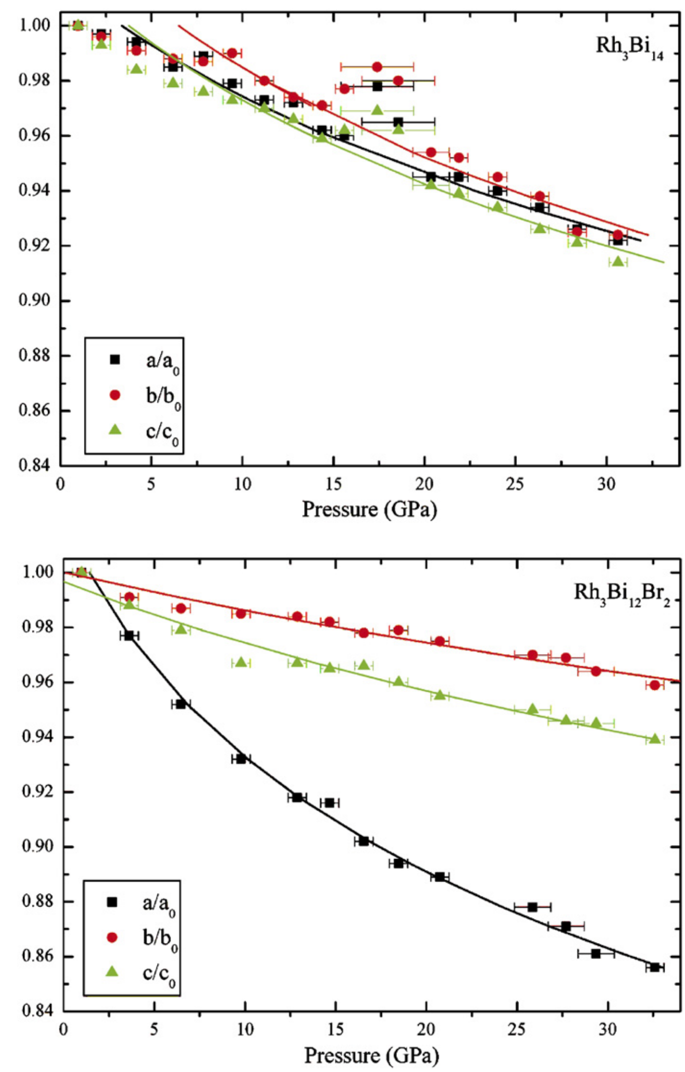

Fig. 9. Relative changes of the lattice parameters of Rh_3Bi_{14} and $Rh_3Bi_{12}Br_2$ as a function of pressure. The solid lines correspond to the fit of a 2nd-order Birch–Murnaghan equation of state on the lattice parameters. The errors of the lattice parameters are in the size of the symbols.

compressibility β_0 is calculated as $\beta_0 = -1/(3K_0) = a_0^{-1}(\partial a/\partial P)_{P=0}$ [13]. The compressibility of *a*–*c* lattice parameters for both compounds are compared in Fig. 9 and Table 4. In Rh_3Bi_{14}, all axes show the same compressibility. In contrast to this, the *b* and *c* axes are less compressible than the *a* axis of $Rh_3Bi_{12}Br_2$ (Fig. 9). This behavior is in good agreement with the bonding analysis. The *b* and *c* axes are mainly controlled by the covalently bonded polycation. The interatomic interactions along the *a* axis include beside the covalent interaction an repulsion between the anions, which seems to be softer and causes the higher compressibility. Despite the behavior of the axes, the volume compressibilities of both phases are equal within the experimental errors. This is not surprising, as the volume compressibility is dominated by the polycationic framework, which is the same for both phases. But the Br atoms in the channels are 'softer' than the Bi atoms, so there is higher compressibility along the channel direction in $Rh_3Bi_{12}Br_2$ than in Rh_3Bi_{14}.

4. Conclusion

The novel intermetallic compound Rh_3Bi_{14} is isostructural with $Rh_3Bi_{12}Br_2$. Both structures consist of the same polycationic framework $[Rh_3Bi_{12}]^{2+}$ built of edge-sharing cubes and square antiprisms of ($RhBi_{8/2}$). In the channels of the polycation the anions Br^{1-} and Bi^{1-} are located. In agreement with the picture of covalent bonding within the polycation, both compounds were found to be stable up to ca. 30 GPa. Caused by the covalent interaction within the polycation, their volume compressibility is equal within the experimental errors. The more soft repulsive interactions between the anions along [100] result in the remarkably larger compressibility of both structures in this direction.

Acknowledgments

Experimental assistances from the staff of the SNBL at ESRF are gratefully acknowledged. This work was supported by the Swiss National Science Foundation (SNF) under contract No. 200021-105233 and carried out within the framework of the Network of Excellence on Complex Metallic Alloys (NoE-CMA) supported by the European Commission within the 6th Framework Program.

References

[1] K. Urban, M. Feuerbacher, J. Non-Cryst. Solids 334&335 (2004) 143.
[2] M.I. McMahon, O. Degtyareva, R.J. Nelmes, Phys. Rev. Lett. 85 (2000) 4896.
[3] M. Ruck, Angew. Chem. Int. Ed. 40 (2001) 1182.
[4] V.P. Glagoleva, G.S. Zhdanov, J. Expt. Theor. Phys. 30 (1956) 248 (Engl. Trans.).
[5] R.G. Ross, W. Hume-Rothery, J. Less, Common Metals 1 (1959) 304.
[6] M. Ruck, Solid State Sci. 3 (2001) 369.
[7] M. Bostrom, S. Hovmoller, J. Solid State Chem. 153 (2000) 398.
[8] Oxford Diffraction Ltd., XCalibur, CrysAlis Software System, Version 1.170, 2003.
[9] G.M. Sheldrick, Program SHELX-97 for crystal structure determination, University of Goettingen, 1997.
[10] R. Miletich, D.R. Allan, W.F. Kuhs, Rev. Min. Geochem. 41 (2000) 445.
[11] A.P. Hammersley, S.O. Svensson, M. Hanfland, A.N. Fitch, D. Häusermann, High Press. Res. 14 (1996) 235.
[12] A.C. Larson, R.B. Von Dreele, LANSCE, MS-H805, Los Alamos National Laboratory, Los Alamos, NM 87545.
[13] R.J. Angel, Rev. Min. Geochem. 41 (2000) 35.
[14] O. Jepsen, A. Burkhardt, O.K. Andersen, The program TB-LMTO-ASA, Version 4.7, Max-Planck-Institut für Festkörperforschung, Stuttgart, 1999.
[15] U. Barth, L. Hedin, J. Phys. C 5 (1972) 1629.
[16] O.K. Andersen, Phys. Rev. B 12 (1975) 3060.
[17] A. Savin, H.J. Flad, J. Flad, H. Preuss, H.G. von Schnering, Angew. Chem. Int. Ed. Engl. 31 (1992) 185.
[18] M. Kohout, Basin, Version 2.3, Max-Planck-Institut für Chemische Physik fester Stoffe, Dresden, 2001.
[19] R.F.W. Bader, Atoms in Molecules: A Quantum Theory, Oxford University Press, Oxford, 1999.
[20] Yu. Grin, U. Wedig, H.G. von Schnering, Angew. Chem. Int. Ed. Engl. 34 (1995) 1204.
[21] M. Kohout, F.R. Wagner, Yu. Grin, Theor. Chem. Acc. 108 (2002) 150.
[22] M. Kohout. Ph.D. Thesis, University of Stuttgart, 1999, p. 14.